Model-based analysis of a twin-screw wet granulation system for continuous solid dosage manufacturing

Ashish Kumar[a,b], Jurgen Vercruysse[c], Séverine T.F.C. Mortier[a,b], Chris Vervaet[c], Jean Paul Remon[c], Krist V. Gernaey[d], Thomas De Beer[b,1], Ingmar Nopens[a,*]

[a] *BIOMATH, Dept. of Mathematical Modelling, Statistics and Bioinformatics, Faculty of Bioscience Engineering, Ghent University, Coupure Links 653, B- 9000 Gent, Belgium*
[b] *Laboratory of Pharmaceutical Process Analytical Technology, Dept. of Pharmaceutical Analysis, Faculty of Pharmaceutical Sciences, Ghent University, Harelbekestraat 72, B-9000 Ghent, Belgium*
[c] *Laboratory of Pharmaceutical Technology, Dept. of Pharmaceutics, Faculty of Pharmaceutical Sciences, Ghent University, Harelbekestraat 72, B-9000 Ghent, Belgium*
[d] *CAPEC-PROCESS Research Center, Dept. of Chemical and Biochemical Engineering, Technical University of Denmark, DK-2800 Kongens Lyngby, Denmark*

[*] Email address: ingmar.nopens@ugent.be, Tel.: +32 (0)9 264 61 96; fax: +32 (0)9 264 62 20
Email addresses: ashish.kumar@ugent.be (Ashish Kumar), jurgen.vercruysse@ugent.be (Jurgen Vercruysse), severine.mortier@ugent.be (Séverine T.F.C. Mortier), chris.vervaet@ugent.be (Chris Vervaet), jeanpaul.remon@ugent.be (Jean Paul Remon), kvg@kt.dtu.dk (Krist V. Gernaey), thomas.debeer@ugent.be (Thomas De Beer)
URL: www.biomath.ugent.be (Ingmar Nopens)
[1] Shared last authorship

Preprint submitted to Computers & Chemical Engineering *March 29, 2016*

Abstract

Implementation of twin-screw granulation in a continuous from-powder-to-tablet manufacturing line requires process knowledge development. This is often pursued by application of mechanistic models incorporating the underlying mechanisms. In this study, granulation mechanisms considered to be dominant in the kneading element regions of the granulator i.e., aggregation and breakage, were included in a one-dimensional population balance model. The model was calibrated using the experimentally determined inflow granule size distribution, and the mean residence time was used as additional input to predict the outflow granule size distribution. After wetting, the first kneading block caused an increase in the aggregation rate which was reduced afterwards. The opposite was observed in case of the breakage rate. The successive kneading blocks lead to a granulation regime separation inside the granulator under certain process conditions. Such a physical separation between the granulation regimes is promising for future design and advanced control of the continuous granulation process.

Keywords: population balance modelling, continuous pharmaceutical production, granule size analysis

1. Introduction

Granulation in the pharmaceutical industry aims at enlarging powder particles, which can be advantageous during the formulation of solid dosage forms (Ennis, 2010). The size enlargement results in gravity forces exceeding the van der Waals forces, thereby contributing to better flow properties required for improved processability and accurate dosing in further downstream processing (Parikh, 2009). Especially in the pharmaceutical industry, where often highly potent drugs are processed, the amount of dust generated by powder handling is reduced by granulation, resulting in improved safety. Also, segregation (demixing) can be minimized along with the improved downstream processing characteristics of the granules.

In the last decade, continuous manufacturing of pharmaceutical solid dosage forms has received great interest due to several process and economic benefits associated with it (Gernaey et al., 2012). A continuous production process can conceptually eliminate scale-up requirements and intermediate storage. With this in mind, twin-screw granulation has emerged as promising method which can be embedded in a continuous manufacturing line which also includes dryer, screening unit and tabletting machine making continuous powder-to-tablet production possible. Moreover, the screws used in the granulator have a modular structure (interchangeable transport and kneading elements) providing flexibility towards adaptation in equipment and process variables depending upon feed characteristics to achieve the required product characteristics.

The available studies have primarily focused on the effect of process variables (such as screw configuration, material throughput, screw speed etc.) (Vercruysse et al., 2012; Dhenge et al., 2011; Thompson and Sun, 2010) and formulation properties (El Hagrasy et al., 2013; Dhenge et al., 2013) on granule properties at the outlet of the twin-screw granulator (TSG) due to the opacity of the multi-phase system in the granulator. Thus, little is known about the effect of these variables on the evolution and kinetics of granule formation in the TSG and the resulting granule structure. In a recent study, granule size distribution (GSD) evolu-

tion along the TSG screw was experimentally mapped in order to understand the dominant constitutive mechanisms of a granulation system such as growth, aggregation and breakage (Kumar et al., 2014a). However, such measurements merely provide a semi-quantitative insight regarding the GSD at discrete time steps, making it difficult to apply in process design applications. Population balance equations (PBEs) are a frequently used mathematical tool to describe particulate processes such as wet granulation (Kumar et al., 2013) and drying of the wet granules (Mortier et al., 2013). An extensive review of the applications of such equations to particulate systems in engineering is given by Ramkrishna (2000). Barrasso et al. (2013) used a multi-component population balance model (PBM) for tracking the liquid content and porosity of each particle size class during the twin-screw granulation. The experimental data reported by El Hagrasy et al. (2013) was used in the study of Barrasso et al. (2013). The data originated from samples collected from the granulator outlet, and therefore a lumped-parameter approach was adopted for the development of the model. Furthermore, Barrasso et al. (2015) applied bi-directional coupling between a particle scale discrete element method (DEM) and PBM for a more mechanistic description of a twin-screw wet granulation process. The model showed sensitivities to the screw configuration, process parameters such as screw speed, liquid-to-solid ratio as well as material properties such as binder viscosity and pore saturation. Although, the bi-directional coupling between DEM and PBM to evaluate collision frequencies and liquid distribution was an excellent proof-of-concept of mechanistic modelling of granulation processes, it is computationally very expensive and requires many particle-scale assumptions, which demand further validation. Due to this, there is still very little understanding regarding the primary driving mechanisms and function of screw components in the twin-screw wet granulation.

In this study, the principal constitutive mechanisms of a granulation system such as growth, aggregation and breakage were included in a PBM framework to track particle size evolution in the different individual screw blocks of a continuous TSG. Based on an

experimentally determined inflow GSD (Kumar et al., 2014a) and mean residence time ($\bar{t}$) (Kumar et al., 2014b) of the granulator, predictions of the outflow GSD were made. The experimental data was used for calibrating the model for individual screw modules in the TSG at different process conditions. The results from the calibrated model were used to understand the role of mixing zones and their locations in the screw under different process conditions.

2. Materials and methods

2.1. Continuous wet-granulation using TSG

Granulation experiments were performed using a 25 mm diameter co-rotating TSG with option to open the barrel, which is the granulation module of the ConsiGma-1 unit (GEA Pharma Systems, Collette™, Wommelgem, Belgium). The TSG consists of a barrel enclosing two co-rotating self-wiping screws. The granulator screws had a length-to-diameter ratio of 20:1. The screw configuration with 6 kneading elements (Length = Diameter/4 for each kneading disc) were composed of one kneading block. For the screw configuration with 12 kneading elements, two kneading blocks each consisting of 6 kneading elements were used (Fig. 1). Both kneading zones were separated by a conveying screw block (Length = 1.5 Diameter). The stagger angle of the kneading elements was fixed at 60°. An extra conveying element (Length = 1.5 Diameter) was implemented after the second kneading block together with 2 narrow kneading elements (Length = Diameter/6 for each kneading disc) in order to reduce the amount of oversized agglomerates, as reported by Van Melkebeke et al. (2008). The barrel jacket temperature was set at 25°C. During processing, the powder premix was gravimetrically fed into the feed segment of the granulator by using a twin-screw feeder with agitator (DDW-MD2-DDSR20, Brabender, Duisburg, Germany). Distilled water as granulation liquid was pumped into the screw chamber using a peristaltic pump (Watson Marlow, Comwall, UK) using silicon tubings connected to two 1.6 mm nozzles,

one for each screw, before the material reaches the mixing zone which contained kneading elements (Fig. 1). The powder was hence wetted by the granulation liquid in this region. Further down, since the granulation occurs by a combination of capillary and viscous forces binding particles in the wet state, the wetted material was distributed, compacted and elongated by the kneading elements of the mixing zones, changing the particle morphology from small (microstructure) to large (macrostructure). It is believed that the material is mixed, compacted and chopped to form irregular and porous granules by the succeeding transport elements and kneading blocks (Vercruysse et al., 2015). The rotation of the screws conveys the material in axial direction through the different zones of the TSG by the drag and flow-induced displacement forces and thus causing mixing and granulation. The rheological behaviour of the material also changes based on liquid-to-solid ratio (L/S) (Althaus and Windhab, 2012).

[Figure 1 about here.]

2.2. Population balance model for TSG

A TSG consists of a wetting zone and several mixing zones containing a finite number of kneading elements, which significantly drive the solid-liquid mixing and hence the granulation process. For the mathematical description of a TSG with two mixing blocks, the compartmentalisation into two well-mixed zones for simulation solved the challenge of inhomogeneous distribution of particle properties along the TSG length. This inhomogeneity exists due to the geometry of the screw as well as the position of the liquid addition ports. The application of compartmentalisation for modelling the inhomogeneity by partitioning the fluidized bed into two different zones was recently presented by Hussain et al. (2014). Introducing an external coordinate can be another possibility to model this inhomogeneity, but that will require implementation of the DEM together with population balances which is computationally more demanding. In order to model the change in GSD across the individual mixing zones, these mixing zones were assumed to be well-mixed systems. The

granulation rate processes which are considered to be dominant in the kneading element regions of the granulator, i.e. aggregation and breakage, were included in a PBM framework (Kumar et al., 2013), which can be represented as:

$$\begin{aligned}\frac{\partial n(t,x)}{\partial t} =& \frac{Q_{in}}{V} n_{in}(x) - \frac{Q_{out}}{V} n_{out}(x) + \frac{1}{2}\int_0^x \beta(t, x-\varepsilon, \varepsilon)\, n(t, x-\varepsilon)\, n(t,\varepsilon)\, d\varepsilon \\ & - n(t,x) \int_0^\infty \beta(t,x,\varepsilon)\, n(t,\varepsilon)\, d\varepsilon + \int_0^\infty b(x,\varepsilon) S(\varepsilon) n(t,\varepsilon)\, d\varepsilon \\ & - S(x) n(x,t)\end{aligned} \tag{1}$$

where, $n(t,x)$ is the number density function of particle size x as the internal coordinate at time t. Here particle size refers to the particle volume. Q_{in} and Q_{out} were inflow and outflow of the material based on throughput and V was the volume of the mixing zone. Assuming the material transport across the mixing zone to occur at a steady state, inflow and outflow can be eliminated from Eq. 1. Moreover, the GSD of the inflow to the second mixing/transport zone was assumed to be identical to the GSD of the outflow from the first mixing zone.

In this study, a sectional method known as the cell average technique (CAT) was applied to solve the PBE (Kumar et al., 2006). It has been shown numerically that CAT is very accurate and efficient, as it prevents over-prediction of number density for the large particles and limits a diverging behaviour of higher moments, which are critically important. The CAT is consistent with the first two moments and the scheme can be generalized to conserve any two moments (Kumar et al., 2006). For this study, the zeroth moment which is proportional to total number of particles and the first moment which is proportional to total mass were calculated.

2.2.1. Aggregation and breakage kernels

The primary challenge for using PBE is to model the kinetics of the twin-screw granulation process in $\beta(t, x, \varepsilon)$ and $b(x, \varepsilon)$, because of their strong dependence on the time and in a fairly complex way on operating parameters and material properties. The aggregation kernel $\beta(t, x, \varepsilon)$ is a product of two factors, aggregation efficiency $\beta_0(t)$ and collision frequency $\beta(x, \varepsilon)$ (Kumar et al., 2013), i.e.,

$$\beta(t, x, \varepsilon) = \beta_0(t)\beta(x, \varepsilon) \tag{2}$$

The aggregation efficiency $\beta_0(t)$ depends on the effect of process and equipment settings on the kinetic energy of particles, their trajectories and several other mechanical properties of the particles such as orientation and surface structure. Often $\beta_0(t)$ is assumed to remain constant with respect to time and size independent (Rao, 2009). The collision frequency $\beta(x, \varepsilon)$ is mostly assumed to be a function of particle size. For the sake of simplicity, the constant aggregation kernel ($\beta(t, x, \varepsilon) = \beta_0$) describing the frequency that particles with diameter ε and $x - \varepsilon$ collide to form a particle of size x was used in this study.

Similar to the aggregation kernel, the breakage kernel is also composed of two components, breakage function $b(x, y)$ and selection function S_0. The breakage function $b(x, y)$ is a probability density function for the formation of particles of size x after breakage of particle of size y. For the breakage process, the quadratic selection function, $S(y) = S_0(y)^\mu$ was used in which S_0 and μ are chosen to be positive rate constants. The breakage function, $b(x, y)$ originally proposed for the ball milling operation by Austin (2002) (eq. 3) was used here. Ball milling is also an operation involving particles in high-shear conditions similar to twin-screw wet granulation, and this breakage function describes the daughter size distribution

x from the breakup of a particle of size y.

$$\beta(x,y) = \frac{\frac{\phi\gamma x^{\gamma-1}}{y^{\gamma}} + \frac{(1-\phi)\alpha x^{\alpha-1}}{y^{\alpha}}}{\frac{\phi\gamma}{\gamma+1} + \frac{(1-\phi)\alpha}{\alpha+1}} \tag{3}$$

where γ, ϕ and α are dimensionless material constants. The term ϕ is called the weight parameter to quantify the mass content of the first breakage distributions. The exponents γ and α represent the width of the fragment distributions ϕ and $1-\phi$, respectively.

2.3. Model parameter estimation

The experimental data provided evidence that the aggregation and breakage are the dominant mechanisms in twin-screw granulation (for details see Kumar et al. (2014b)) and a model framework was developed to include these phenomena. However, various parameters in this model are unknown and can vary based on process settings and material properties. Experimental data of GSD of granule samples from various locations inside the granulator (Fig. 1) were used to estimate values of five model parameters: three dimensionless material constants, γ, ϕ and α and the aggregation constant β_0 and the selection function constant S_0. Based on available literature, the selection function constant μ was fixed at 0.33 (Gokhale et al., 2009). The estimation of these parameters was done by minimising the root mean square error (RMSE) as an objective function (eq. 4):

$$\mathrm{RMSE} = \sqrt{\frac{\sum_{i=1}^{I}(\mathrm{N}_{\mathrm{sim},i} - \mathrm{N}_{\mathrm{exp},i})^2}{n}} \tag{4}$$

where $\mathrm{N}_{\mathrm{sim},i}$ and $\mathrm{N}_{\mathrm{exp},i}$ are the simulated and experimentally measured number density values for I bins of the granule size range. In order to find the global minimum of the objective function, the "brute force" method was used, which computed the objective function's value at each point of a multi-dimensional grid of points, to arrive at the global minimum of the function. This multidimensional grid contained physically sound ranges of β_0 (1e-5,

0.4), S_0 (0.001, 3.5), α (3.3e-6, 1), γ (1.6e-4, 5) and ϕ (0.01, 1.5) with linear step length of 0.005, 0.005, 0.000005, 0.05 and 0.05, respectively. Later, to obtain a more precise (local) minimum, the downhill simplex algorithm was used applying the estimation result of brute force minimization as initial guess (Nelder and Mead, 1965). The estimated parameter ranges from brute force minimization were also useful to check any correlations between estimated parameters, as well as to determine the confidence interval of the fitted parameters using bootstrap estimation (Efron and Tibshirani, 1986). In the Bootstrap estimation 25 randomly picked residuals R_{syn} from the least RMSE fitting using estimated parameters was used to generate 50 synthetic datasets from the experimental data N_{exp}, such that

$$N_{syn,i} = N_{exp,i} + R_{syn,i} \tag{5}$$

The $N_{syn,i}$ was again fitted using the same algorithm which minimises the RMSE for the actual experimental data $N_{exp,i}$ as discussed before. The 50 bootstrap parameter sets thus obtained were used to calculate the 95% confidence interval (CI) as,

$$CI_{95\%} = \mu \pm 1.96\sigma \tag{6}$$

by calculating the mean μ and standard deviation σ of each parameter in the bootstrap parameter sets. The implementation of the PBM solution method, model parameter estimation and bootstrap estimation were performed using Python which is a simple yet powerful programming language, employing built-in functions in scientific libraries NumPy and SciPy (Oliphant, 2007).

2.4. GSD experimental data for model calibration

The granulation data was obtained by granulating a premix of α-Lactose monohydrate (Pharmatose 200M, Caldic, Hemiksem, Belgium) and Polyvinylpyrrolidone (PVP)

(Kollidon® 30, BASF, Ludwigshafen, Germany) (ratio: 97.5/2.5, w/w) with distilled water.

The experiments were performed to evaluate the influence of the number of mixing zones with kneading elements (1×6 and 2×6), high and low level screw speed (500 and 900 rpm), at a high throughput (25 kg/h) and L/S (6.72% (w/w) based on wet mass). For each run, samples were collected from different locations inside the barrel by opening the barrel after stopping the process running at steady state (Fig. 1). Sample location 1 was just prior to the first kneading block, sample location 2 on the first kneading block, sample location 3 was between the first and second kneading block, sample locations 4 and 5 were on and right after the second kneading block. Irrespective of the number of kneading blocks, sample locations on the screw were kept constant during sampling. The wet granules from all the experiments were dried at room temperature for 24 h to measure the GSD of the sample.

2.4.1. Dynamic image analysis for granule size measurement

The GSD of the samples from sampling locations 1, 3 and 5 which were inside the TSG barrel (Fig. 1), were determined via dynamic image analysis (DIA) used in the EyeTech instrument (Ankersmid B.V., Oosterhout, The Netherlands). A high speed camera records pictures (up to 30 pictures /sec) and visualises the particle distribution in real time during the measurement. The camera was synchronized with a pulsing light emitting diode (LED) and takes backlighted images. The captured images of flowing powders were used to calculate the average Feret diameter of the granules. Complete number based GSD (Q_0) was used for the model calibration. The GSD span is presented as quantiles 25%, 50% and 75%, thus a shift in the quartiles indicated a change in a certain size fraction and dominance of the related constitutive mechanism.

Detailed reasoning regarding the sample locations and measurement methods, and GSD trends at different settings can be obtained in the related experimental study by Kumar et al. (2014b). To incorporate the time along with the granule size measurement data, the mean residence time ($\bar{t}$) of the granulator was experimentally obtained at different process

settings by Kumar et al. (2014b). For each transport and mixing zone of a process setting, the simulation time was $\frac{\bar{t}}{3}$.

2.5. Parameter estimation for predictive modelling

Both for the screw configuration with 1×6 and 2×6 kneading elements, for the runs at low (500 rpm) and high (900 rpm) screw speed, the experimentally measured GSD from location 1, 3 and 5 in Fig. 1 were used for model calibration. In order to quantitatively represent these trends in the simulations, the unknown rate parameters of the aggregation and Austin breakage kernels were estimated by comparing the simulation results with experimental data. The estimated model parameters and their confidence interval (95%) estimates for the simulation of a granulator with one mixing zone at low (500 rpm) and high (900 rpm) screw speeds are listed in table 1. The error estimates (RMSE and R^2) are mentioned in Fig. 3 and 4. Furthermore, the estimated parameters for the numerical computations and their confidence intervals (95%) for a granulator with two mixing zones at low (500 rpm) and high (900 rpm) screw speeds are listed in table 2.

Table 1: Estimated model parameters with corresponding confidence intervals (95%) at low (500 rpm) and high (900 rpm) screw speeds and for one mixing zone followed by the transport zone (II) of the granulator.

Screw speed	Low (500 rpm)		High (900 rpm)	
Zone	Mixing	Transport	Mixing	Transport
β_0	1.05E-03 ± 1.17E-04	3.12E-01 ± 1.16E-02	2.36E-04 ± 4.07E-05	2.95E-01 ± 1.19E-02
S_0	3.01E-02 ± 2.18E-03	3.30E+00 ± 3.18E-01	5.10E-02 ± 2.25E-03	1.18E+00 ± 2.37E-02
α	6.01E-02 ± 5.53E-06	1.65E-07 ± 1.94E-08	1.86E-04 ± 4.49E-06	1.14E-06 ± 9.30E-07
γ	5.21E-01 ± 8.07E-02	4.24E-01 ± 1.19E-03	8.28E-01 ± 1.31E-02	3.07E-01 ± 3.13E-03
ϕ	9.73E-01 ± 4.51E-02	7.20E-01 ± 6.54E-03	4.07E-01 ± 2.98E-03	5.34E-01 ± 7.29E-03

The low RMSE and high R^2 values for all the screw speeds and mixing zones (Fig. 3 and 4) indicate that numerical results were in excellent agreement with the experimental data for each location inside the granulator. As an example, Fig. 2 illustrates the fit between simulated and experimental GSD for the screw configuration with two mixing zones (I, II) of the granulator operated at a low screw speed. However, the solutions were subject to

different optimal model parameters for each section. This suggests that the different sections of the granulator behave differently when the process conditions are varied.

Table 2: Estimated model parameters with corresponding confidence intervals (95%) at different screw speeds and for two mixing zones (I, II) of the granulator.

Screw speed	Low (500 rpm)		High (900 rpm)	
Zone	Mixing I	Mixing II	Mixing I	Mixing II
β_0	3.02E-03 ± 1.47E-04	1.95E-01 ± 4.56E-02	8.97E-02 ± 3.36E-03	4.99E-02 ± 1.80E-02
S_0	2.53E-02 ± 5.91E-03	7.99E-01 ± 4.35E-02	3.11E-02 ± 2.25E-03	5.72E-01 ± 3.55E-02
α	1.13E-05 ± 8.83E-06	6.11E-01 ± 3.19E-02	1.26E-03 ± 3.29E-04	4.38E-01 ± 9.30E-02
γ	4.05E+00 ± 7.60E-01	3.81E-03 ± 2.18E-04	2.63E-01 ± 9.02E-03	4.49E-02 ± 3.78E-03
ϕ	1.03E+00 ± 2.31E-01	5.43E-02 ± 2.24E-03	1.18E+00 ± 3.89E-01	1.50E-02 ± 2.13E-03

[Figure 2 about here.]

3. Results and discussion

3.1. Simulated dynamic behaviour in the mixing zones of the TSG

3.1.1. Screw configuration with one mixing zone

In this process condition, the mixing zone was placed between location 1 and 3. So, the downstream material from the mixing zone was conveyed between location 3 and 5 by the transport elements without any further distributive mixing by the kneading elements.

At a low screw speed

The simulation results for a screw configuration with one mixing zone showed that at a low screw speed, the mixing zone between location 1 and 3 was mainly involved in breakage of over-wetted lumps after the wetting of the powder immediately before location 1 (Fig. 3.a). This was indicated by the sharp reduction in the D_{75} of the simulated dynamic trends of the GSD. The D_{50} remained fairly constant and the D_{25} increased slightly when the material passed the first mixing zone. As the fill ratio is high due to the high throughput (25 kg/h) and the low screw speed (500 rpm), the mechanical shear and distributive mixing by the kneading elements caused breakage of over-wetted lumps.

In the subsequent section with transport elements (between location 3 and 5), the material was conveyed, but was only slightly mixed (Fig. 3.b). This led to a minor reduction in the oversized fraction. However, no further change in the other fractions was observed. After an initial slight reduction, all the quartile values of the GSD remained constant as the material passed the first mixing zone. This suggests that without mechanical mixing further granulation cannot be achieved under these process conditions.

[Figure 3 about here.]

At a high screw speed

When the screw speed is increased from 500 to 900 rpm the fill ratio inside the barrel is reduced (Fig. 3.c). In the simulation of the high screw speed condition, this was reflected in a more uniform change in GSD. The larger over-wetted lumps broke when the material passed the first mixing zone. This was reflected by reduction in the D_{75} of the simulated dynamic trends of the GSD. Moreover, the D_{50} and the D_{25} values increased slightly which indicated an improved granulation compared to that achieved at a low screw speed. This also suggests that conditions favouring very high filling of the barrel are desirable for the twin-screw granulation process.

In the subsequent section of the TSG, despite the fact that mechanical mixing by the kneading discs was not present between location 3 and location 5, the higher shear due to increased screw speed resulted in further granulation as inferred (Fig. 3.d). Therefore, there was little increase in the D_{25} values between location 3 and location 5. Moreover, some breakage of the oversized fraction occurred, as indicated by the reduction in the D_{75} value of the dynamic GSD trend.

3.1.2. Screw configuration with two mixing zones

At a low screw speed

The simulation results for a screw configuration with two mixing zones showed that when the screw speed was low (Fig. 4.a), the D_{75} remained constant whereas the D_{25} and D_{50} increased when the material passed the first mixing zone. This indicates that the primary role of the first kneading block at this condition was supporting the aggregation leading to formation of larger granules. The second mixing zone at this condition caused breakage of the larger granules leading to reduction in D_{50} as well together with D_{75} (Fig. 4.b). However, the D_{25} value of the GSD increased by the mixing in the second zone at this condition. This suggests a mixed regime in the second mixing zone of the TSG where both aggregation and breakage compete with each other. This situation is similar to higher shear mixers where granulation regimes co-exist and thus it is difficult to control granulation. Moreover, the barrel at this condition was highly filled due to the low screw conveying rate at low screw speed leading to less space for material to get distributed. This was also the reason why in the experimental study this condition led to an undesirably high level of torque (Kumar et al., 2014b).

[Figure 4 about here.]

At a high screw speed

The simulation of the high screw speed condition showed a significant change in the granulation behaviour in the two mixing zones (Fig. 4.c and d). Unlike the case with low screw speed, when the material passed through the first mixing zone at this condition all the quartiles of the GSD increased (Fig. 4.c). This indicates that aggregation was the most dominant mechanism under these conditions in this mixing zone, while the level of breakage was very low leading to no reduction in any fraction with time. However, when the material was introduced to the second kneading block, the quartile values D_{75} and D_{50}

dropped significantly, which indicates that breakage occurred as the dominant mechanism in the second mixing zone (Fig. 4.d). This observation by process simulation is very important as it established that the successive kneading blocks led to a granulation regime-separation inside the twin-screw granulator under this condition. The mixing of the wetted powder in the first kneading block caused an increase in the aggregation rate, which was reduced after the second kneading block. However, the breakage rate increased successively along the length of the granulator. Such a physical separation between the granulation regimes is promising for future design of the granulation system. Moreover, a properly calibrated and validated model for such a condition can be used to study the designing of advanced control system for the continuous granulation process.

4. Computation time, efficiency and accuracy

In the present study, where off-line calculations were performed for knowledge development, simulation time was not as critical. However, the computational efficiency both in terms of simulation time and accuracy of the numerical schemes is very important for more diverse applications.

Therefore, the solution time, accuracy and computational memory requirement of the current scheme was compared for different grid sizes to test the efficiency and suitability (Table 3). It was observed that increasing the number of bins from 10 to 30 increased the accuracy of prediction with minor increase in the computational time ($\sim$1.4 times more than 10 grids) and memory requirement ($\sim$1.1 times more than 10 grids). An increase in the number of bins from 30 to 50 resulted in minor improvement in the accuracy but resulted in further increase in the computational time ($\sim$1.4 times more than 30 bins) and no increase in the memory requirement. However, further increase in the number of bins up to 100 bin resulted in both an increase in the computational time ($\sim$2.4 times more than 50 bins) and a reduction in the accuracy in several cases. This is mainly because the insufficient samples

per bin in the refined grid caused large statistical fluctuations that resulted in substantial inaccuracies in the probability densities of the experimentally measured GSD. Thus, the bin width should be kept sufficiently large to ensure that a sufficient number of sampled particles are measured for each bin and the chance of statistical error is minimised. This is a particularly important consideration for the real-time optimization and control simulations where the state vector of probability density of the GSD relies on the small sampling time window during the continuous monitoring of granules from the process.

Table 3: Change in the computation time (s), accuracy [RMSE] (µm) and memory requirement [MR] (MB) with refinement of the grid for PBM solution at different screw speeds and with one and two mixing zones. Computational settings which have been used to generate the results presented in section 3.1 has been highlighted with italic text.

	Screw		10 grid			30 grid			*50 grid*			100 grid		
	speed	Zone	RMSE	time	MR	RMSE	time	MR	*RMSE*	*time*	*MR*	RMSE	time	MR
1 mixing zone	Low	Mixing	5.42	5.08	95.1	5.32	6.14	133.0	*5.26*	*9.63*	*134.2*	5.22	19.27	136.9
		Transport	2.65	5.42	115.8	2.35	8.98	133.0	*2.32*	*13.92*	*136.3*	2.33	36.32	137.7
	High	Mixing	8.91	5.17	125.4	4.65	6.07	132.8	*4.36*	*7.70*	*136.2*	4.21	17.77	138.0
		Transport	6.95	5.34	125.4	3.46	7.91	132.8	*3.47*	*11.16*	*136.2*	3.47	29.89	138.0
2 mixing zones	Low	Mixing 1	12.76	5.75	122	7.61	7.53	133.0	*7.33*	*11.90*	*136.3*	7.47	18.60	137.7
		Mixing 2	7.24	5.66	122.1	2.48	7.69	132.8	*2.44*	*9.45*	*136.2*	2.50	22.08	138.0
	High	Mixing 1	31.85	5.24	125.7	23.62	8.40	132.8	*18.28*	*13.76*	*136.2*	19.70	34.44	138.0
		Mixing 2	3.80	5.42	130.4	3.79	8.21	133.1	*3.77*	*12.73*	*136.2*	3.74	37.77	138.0

5. Model application and future development

As per the results shown above, it is concluded that the proposed PBM framework can be used for building improved process knowledge regarding the mixing zones of the continuous twin-screw granulation process at steady-state. Also, it was established by the discretised PBM that the process and equipment variables were linked to the time evolution of the GSD in the TSG. The results from the calibrated model also elucidated the regime-separation phenomena under certain process conditions. This hints towards a potential decomposition of the twin-screw granulation system, allowing to simulate the complete granulator by switching between different granulation mechanisms.

Besides, an application model is required which completely captures the essential dynamics involved in the full length of the twin-screw granulation process. To completely describe the granulator dynamics, the coupling between two PBMs for individual mixing blocks, i.e. a two-stage granulator model is required. The model used in this study was a one-dimensional (i.e. considering granule size only) PBM (eq. 1) limited to one stage only, and the experimental data was used to extract the aggregation and breakage rates for individual blocks of the granulator at a certain condition (Table 1 and 2). Therefore, the link between process variables and the constant parameters of the rate kernels needs to be explored, which can be used to predict the result of the granulation process within the experimental window of the design of experiments used for the parameter estimation (Sanders et al., 2009).

Furthermore, in order to further improve the model, future work should focus on introducing the wetting kinetics in the model framework and to obtain particle flux data and collision frequencies using DEM to avoid the parameter estimation by model inversion. Additionally, dedicated mechanistic kernels for the twin-screw granulation can be developed in order to improve the sensitivity of the model towards the change in process conditions and other field parameters. Finally, a validated model can be used to define the design space of the process for the future optimization and model-based design of a control system of the granulation process.

6. Conclusions

A 1-D PBM including aggregation and breakage subprocesses for a continuous twin-screw granulation process was presented. Unknown model parameters and their 95% confidence range were estimated using experimentally measured particle size distributions from inside the granulator. The calibrated model was then used as a predictive tool within the experi-

mental space. The results showed strong agreement with experimental data. This approach is the better way forward for the development of twin-screw granulation models as multiple factors of the twin-screw granulator leading to an experimental output can now constrain the model during calibration. Further analysis revealed that, at high screw speed, the successive kneading blocks can lead to the dominance of different constitutive granulation mechanisms inside the twin-screw granulator. The ability to achieve a physical separation between the granulation regimes inside the granulator can be promising for future design and advanced control of the continuous granulation process using the twin-screw granulator. Furthermore, the study suggested that a model-based approach can be adopted to develop a better understanding of twin-screw granulation processes. A validated model can ultimately be used to define the design space of the process to facilitate process optimization and model-based control.

Acknowledgements

Financial support for this research from the BOF (Bijzonder Onderzoeksfonds Universiteit Gent, Research Fund Ghent University) is gratefully acknowledged.

Appendix A. Numerical solution of PBM

In this study, a sectional method known as the CAT was applied to solve the PBE (Kumar et al., 2006). The numerical solution scheme can be briefly described as follows:

(i) *Domain discretisation*: First, the computational domain $]0, d_{max}]$ is fixed and the truncated equation is obtained from eq. 1 by replacing ∞ by d_{max}. In order to accommodate particles of a wide size range with a minimal number of bins, a logarithmic grid with $I = 50$ bins was used for the discretisation of internal coordinates, such that bin $\Delta_i :=]d_{i-1/2}, d_{i+1/2}]$, where $i = 1, ..., I$, with $d_{I+1/2} = 3000$ µm, which is the maximum granule size under consideration for this study. The *pivot* for each bin is calculated as

the arithmetic mean $d_i = (x_{i-1/2} + x_{i+1/2})/2$, where the particle distributions within bin Δ_i are considered to be represented by a point mass. According to the mid-point rule, they are second order quadrature points.

(ii) *Computation of birth and death rates*: The discrete events such as aggregation and breakage, which can occur at arbitrary locations in the discretised domain, lead to a change in the particle size and adds or removes particles in the ith bin of the domain. The latter phenomena of adding or removing particles from a bin are termed as birth and death, respectively. Since both aggregation and breakage processes are considered to take place together in the mixing zones, the discrete birth and death rates for the combined processes are considered by algebraically summing the total birth and death rates in a bin, i.e.,

$$\begin{aligned}\frac{dN_i}{dt} &= B^{mod}_{agg,i} + B^{mod}_{break,i} - D_{agg,i} - D_{break,i} \\ &= B^{mod}_{agg+break,i} - D_{agg+break,i}\end{aligned} \tag{7}$$

where $B^{mod}_{agg+break,i}$ and $D^{mod}_{agg+break,i}$ represent the modified birth and death rates of particles in the ith bin due to aggregation and breakage respectively. The discrete birth and death rates can be obtained by substituting a Dirac-delta representation of the number density $n(t,x) \approx \sum_{i=1}^{I} N_i \delta(x - x_i)$ into the continuous form of total birth and death rates in each bin. Thereby $B_{agg,i}$, $B_{break,i}$, $D_{agg,i}$, $D_{break,i}$ are calculated as :

$$B_{agg,i} = \sum_{\substack{j,k \\ x_{i-1/2} \le (x_j + x_k) < x_{i+1/2}}}^{j \ge k} (1 - \frac{1}{2}\delta_{j,k} N_j N_k) \tag{8}$$

The net flux of volume $V_{agg,i}$ into the ith bin as a result of aggregations between

particles is therefore given by

$$V_{agg,i} = \sum_{\substack{j,k \\ x_{i-1/2} \leq (x_j + x_k) < x_{i+1/2}}}^{j \geq k} (1 - \frac{1}{2}\delta_{j,k} N_j N_k)(x_j + x_k) \tag{9}$$

The death rate, $D_{agg,i}$ is calculated as:

$$D_{agg,i} = N_i \sum_{k=1}^{I} \beta_{i,k} N_k \tag{10}$$

The discrete birth $B_{break,i}$ and death $D_{break,i}$ due to breakage events in the ith bin are computed by the following expressions:

$$B_{break,i} = \sum_{k \geq i} N_k(t) S_k \int_{x_{i-1/2}}^{p_k^i} b(x, x_k) \tag{11}$$

and,

$$D_{break,i} = S_i N_i(t) \tag{12}$$

where, p_k^i is defined as

$$p_k^i = \begin{cases} x_i, & \text{if } k = i \\ x_{i+1/2} & \text{otherwise} \end{cases} \tag{13}$$

Similar to the net flux of volume $V_{agg,i}$, the discrete volume flux in the ith bin due to birth by breakage is given by

$$V_{break,i} = \sum_{k \geq i} N_k(t) S_k \int_{x_{i-1/2}}^{p_k^i} x b(x, x_k) dx \tag{14}$$

The total birth and death rates in the ith bin are then calculated as

$$B_{agg+break,i} = B_{agg,i} + B_{break,i} \tag{15}$$

and,

$$D_{agg+break,i} = D_{agg,i} + D_{break,i} \tag{16}$$

(iii) *Computation of average volume in bins*: For the consistency of two moments, the net birth in the ith bin is calculated using the volume average of all newborn particles due to aggregation and breakage within three neighbouring bins, $(i-1)$th, ith and $(i+1)$th. Thus, the average volume of the particles in each bin is calculated as

$$\bar{v}_i = \frac{V_{agg,i} + V_{break,i}}{B_{agg,i} + B_{break,i}} \tag{17}$$

If the average volume $\bar{v}_i$ matches with the respective size of the bin x_i then the total birth B_i can directly be assigned to the node x_i. However, this is rarely possible and hence the total particle birth $B_{agg+break,i}$ is reassigned based on the position of the average value to the neighbouring nodes such that the total number and mass remain conserved.

(iv) *Birth modification*: As the volumes of the newborn particles due to aggregation and/or breakage may lie between the bins of the logarithmic grid, the CAT allocates these particles into the corresponding bins. The modified birth term for this purpose is calculated

$$\begin{aligned} B^{mod}_{agg+break,i} =& B_{agg+break,i-1}\lambda_i^-(\bar{v}_{i-1})H(\bar{v}_{i-1} - x_{i-1}) \\ &+ B_{agg+break,i}\lambda_i^-(\bar{v}_i)H(x_i - \bar{v}_i) \\ &+ B_{agg+break,i}\lambda_i^+(\bar{v}_i)H(\bar{v}_i - x_i) \\ &+ B_{agg+break,i-1}\lambda_i^+(\bar{v}_{i+1})H(x_{i+1} - \bar{v}_{i+1}) \end{aligned} \tag{18}$$

where, the discontinuous Heaviside step function H is defined as

$$H = \begin{cases} 1, & \text{if } x > 0 \\ 1/2 & \text{if } x = 0 \\ 0 & \text{if } x < 0 \end{cases} \tag{19}$$

and the function used for the distribution of particles is given as

$$\lambda^{\pm}(x) = \frac{x - x_{i\pm1}}{x_1 - x_{i\pm1}} \tag{20}$$

Thus, the modified birth rate $B^{mod}_{agg+break,i}$ is consistent with the first two moments. There is no need to modify the death term since particles are just removed from the grid points and therefore the formulation remains consistent with all moments due to discrete death $D_{agg+break,i}$.

(v) *Solving ordinary differential equations (ODEs)*: The values of $B^{mod}_{agg+break,i}$ and $D_{agg+break,i}$ were substituted in eq. 7. The obtained set of ODEs was solved simultaneously for each bin using the higher order LSODE (Livermore Solver for Ordinary Differential Equations) routine from the Odespy package (Langtangen and Wang, 2014). The LSODE is an adaptive solver based on a variable order backward differentiation formulas (BDF) code, allowing order specification. So, the maximum order was specified as 5 and the time steps were getting adjusted throughout the solution process to meet the prescribed absolute error tolerance (1×10^{-6}) .

Glossary

β Aggregation kernel [m^3s^{-1}].

CAT cell average technique.

DEM discrete element method.

DIA dynamic image analysis.

GSD granule size distribution.

L/S liquid-to-solid ratio.

LED light emitting diode.

$n(x,t)$ Number distribution of particles [-].

ODE ordinary differential equation.

PBE population balance equation.

PBM population balance model.

RMSE root mean square error.

S Selection function [s^{-1}].

$\bar{t}$ Mean residence time, [s].

TSG twin-screw granulator.

x Scalar-state variable such as particle size [m, m^3].

References

Althaus, T. O., Windhab, E. J., Jan 2012. Characterization of wet powder flowability by shear cell measurements and compaction curves. Powder Technol. 215-216, 59–65.

Austin, L. G., 2002. A treatment of impact breakage of particles. Powder Technol. 126 (1), 85 – 90.

Barrasso, D., Eppinger, T., Pereira, F. E., Aglave, R., Debus, K., Bermingham, S. K., Ramachandran, R., 2015. A multi-scale, mechanistic model of a wet granulation process using a novel bi-directional PBM-DEM coupling algorithm. Chem. Eng. Sci. 123 (0), 500 – 513.

Barrasso, D., Walia, S., Ramachandran, R., 2013. Multi-component population balance modeling of continuous granulation processes: A parametric study and comparison with experimental trends. Powder Technol. 241 (0), 85 – 97.

Dhenge, R. M., Cartwright, J. J., Doughty, D. G., Hounslow, M. J., Salman, A. D., 2011. Twin screw wet granulation: Effect of powder feed rate. Adv. Powder Technol. 22 (2), 162 – 166.

Dhenge, R. M., Washino, K., Cartwright, J. J., Hounslow, M. J., Salman, A. D., 2013. Twin screw granulation using conveying screws: Effects of viscosity of granulation liquids and flow of powders. Powder Technol. 238, 77–90.

Efron, B., Tibshirani, R., 1986. Bootstrap methods for standard errors, confidence intervals, and other measures of statistical accuracy. Stat. Sci. 1 (1), pp. 54–75.

El Hagrasy, A. S., Hennenkamp, J. R., Burke, M. D., Cartwright, J. J., Litster, J. D., 2013. Twin screw wet granulation: Influence of formulation parameters on granule properties and growth behavior. Powder Technol. 238, 108–115.

Ennis, B. J., 2010. Theory of Granulation: An Engineering Perspective. In: Handbook of Pharmaceutical Granulation Technology. pp. 6–58.

Gernaey, K. V., Cervera-Padrell, A. E., Woodley, J. M., 2012. A perspective on PSE in pharmaceutical process development and innovation. Comput. Chem. Eng. 42, 15–29.

Gokhale, Y., Kumar, R., Kumar, J., Hintz, W., Warnecke, G., Tomas, J., 2009. Disintegration process of surface stabilized sol-gel nanoparticles by population balances. Chem. Eng. Sci. 64 (24), 5302 – 5307.

Hussain, M., Kumar, J., Peglow, M., Tsotsas, E., 2014. On two-compartment population balance modeling of spray fluidized bed agglomeration. Comp. Chem. Eng. 61 (0), 185 – 202.

Kumar, A., Gernaey, K. V., De Beer, T., Nopens, I., 2013. Model-based analysis of high shear wet granulation from batch to continuous processes in pharmaceutical production – a critical review. Eur. J. Pharm. Biopharm. 85 (3, Part B), 814 – 832.

Kumar, A., Vercruysse, J., Bellandi, G., Gernaey, K. V., Vervaet, C., Remon, J. P., Beer, T. D., Nopens, I., 2014a. Experimental investigation of granule size and shape dynamics in twin-screw granulation. Int. J. Pharm. 475 (1-2), 485 – 495.

Kumar, A., Vercruysse, J., Toiviainen, M., Panouillot, P.-E., Juuti, M., Vanhoorne, V., Vervaet, C., Remon,

J. P., Gernaey, K. V., De Beer, T., Nopens, I., 2014b. Mixing and transport during pharmaceutical twin-screw wet granulation: Experimental analysis via chemical imaging. Eur. J. Pharm. Biopharm. 87 (2), 279 – 289.

Kumar, J., Peglow, M., Warnecke, G., Heinrich, S., Morl, L., 2006. Improved accuracy and convergence of discretized population balance for aggregation: The cell average technique. Chem. Eng. Sci. 61 (10), 3327–3342.

Langtangen, H. P., Wang, L., 2014. Odespy software package. `https://github.com/hplgit/odespy`.

Mortier, S. T. F. C., Gernaey, K. V., De Beer, T., Nopens, I., 2013. Development of a population balance model of a pharmaceutical drying process and testing of solution methods. Comp. Chem. Eng. 50, 39 – 53.

Nelder, J. A., Mead, R., 1965. A simplex method for function minimization. Comput. J. 7 (4), 308–313.

Oliphant, T. E., 2007. Python for scientific computing. Comp. Sci. Eng. 9 (3), 10–20.

Parikh, D. M., 2009. Introduction. In: Handbook of Pharmaceutical Granulation Technology. pp. 1–5.

Ramkrishna, D., 2000. Population balances: Theory and applications to particulate systems in engineering. Academic press.

Rao, N. N., 2009. Simulations for modelling of population balance equations of particulate processes using the discrete particle model (DPM). Ph.D. thesis, Otto-von-Guericke-Universität Magdeburg, Universitätsbibliothek.

Sanders, C. F. W., Hounslow, M. J., Doyle, F. J., 2009. Identification of models for control of wet granulation. Powder Technol. 188 (3), 255–263.

Thompson, M. R., Sun, J., 2010. Wet granulation in a twin-screw extruder: Implications of screw design. J. Pharm. Sci. 99 (4), 2090–2103.

Van Melkebeke, B., Vervaet, C., Remon, J. P., 2008. Validation of a continuous granulation process using a twin-screw extruder. Int. J. Pharm. 356 (1-2), 224–230.

Vercruysse, J., Burggraeve, A., Fonteyne, M., Cappuyns, P., Delaet, U., Assche, I. V., Beer, T. D., Remon, J., Vervaet, C., 2015. Impact of screw configuration on the particle size distribution of granules produced by twin screw granulation. Int. J. Pharm. 479 (1), 171 – 180.

Vercruysse, J., Córdoba Díaz, D., Peeters, E., Fonteyne, M., Delaet, U., Van Assche, I., De Beer, T., Remon, J. P., Vervaet, C., 2012. Continuous twin screw granulation: Influence of process variables on granule and tablet quality. Eur. J. Pharm. Biopharm. 82 (1), 205–211.

List of Figures

1 TSG screws with two mixing zones, each containing six kneading elements. Numbers indicate experimental sampling locations used for model calibration. 28

2 Fit between simulated and experimental granule size distribution for a TSG with two mixing zones (I, II) of the granulator at low screw speed. 29

3 Experimental (•) and simulated (—) trends for dynamic changes in quartiles of the GSD (D_{25}, D_{50}, D_{75}) at low (a and b) and high (c and d) screw speeds for the mixing zone (a and c) and transport zone (b and d) of the TSG. . . . 30

4 Experimental (•) and simulated (—) trends for dynamic changes in quartiles of the GSD (D_{25}, D_{50} and D_{75}) at low (a and b) and high (c and d) screw speeds for first (a and c) and second (b and d) mixing zones of the TSG. . . 31

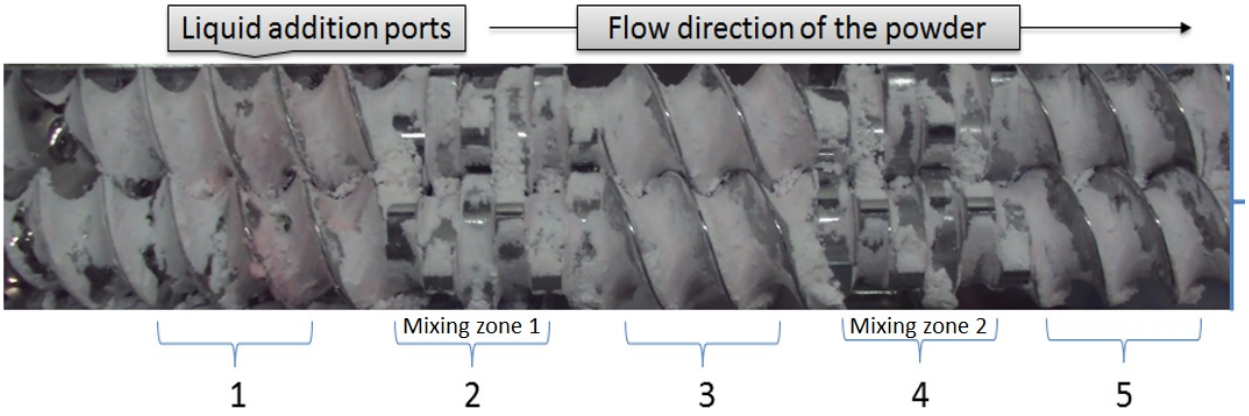

Figure 1: TSG screws with two mixing zones, each containing six kneading elements. Numbers indicate experimental sampling locations used for model calibration.

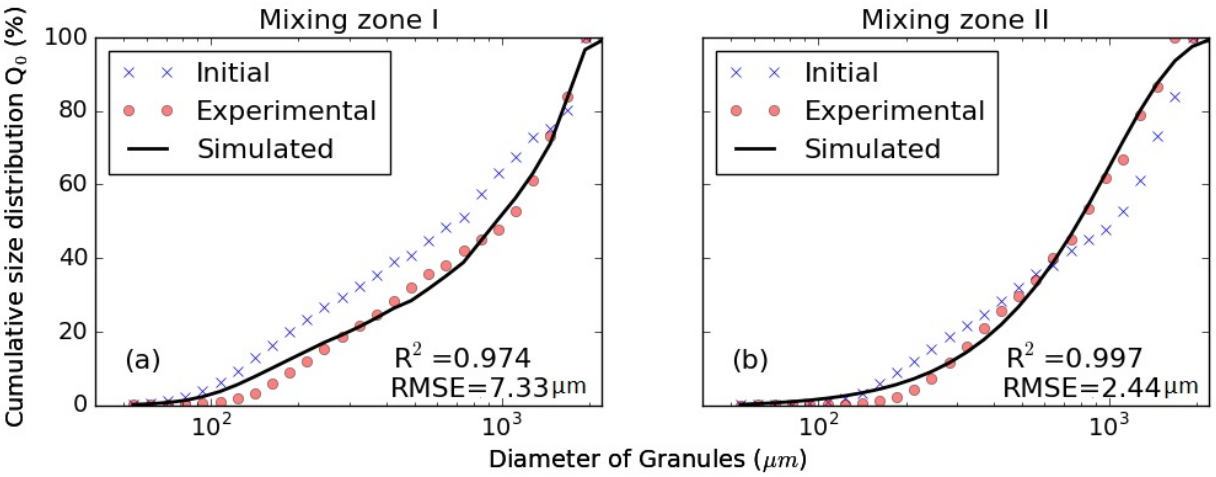

Figure 2: Fit between simulated and experimental granule size distribution for a TSG with two mixing zones (I, II) of the granulator at low screw speed.

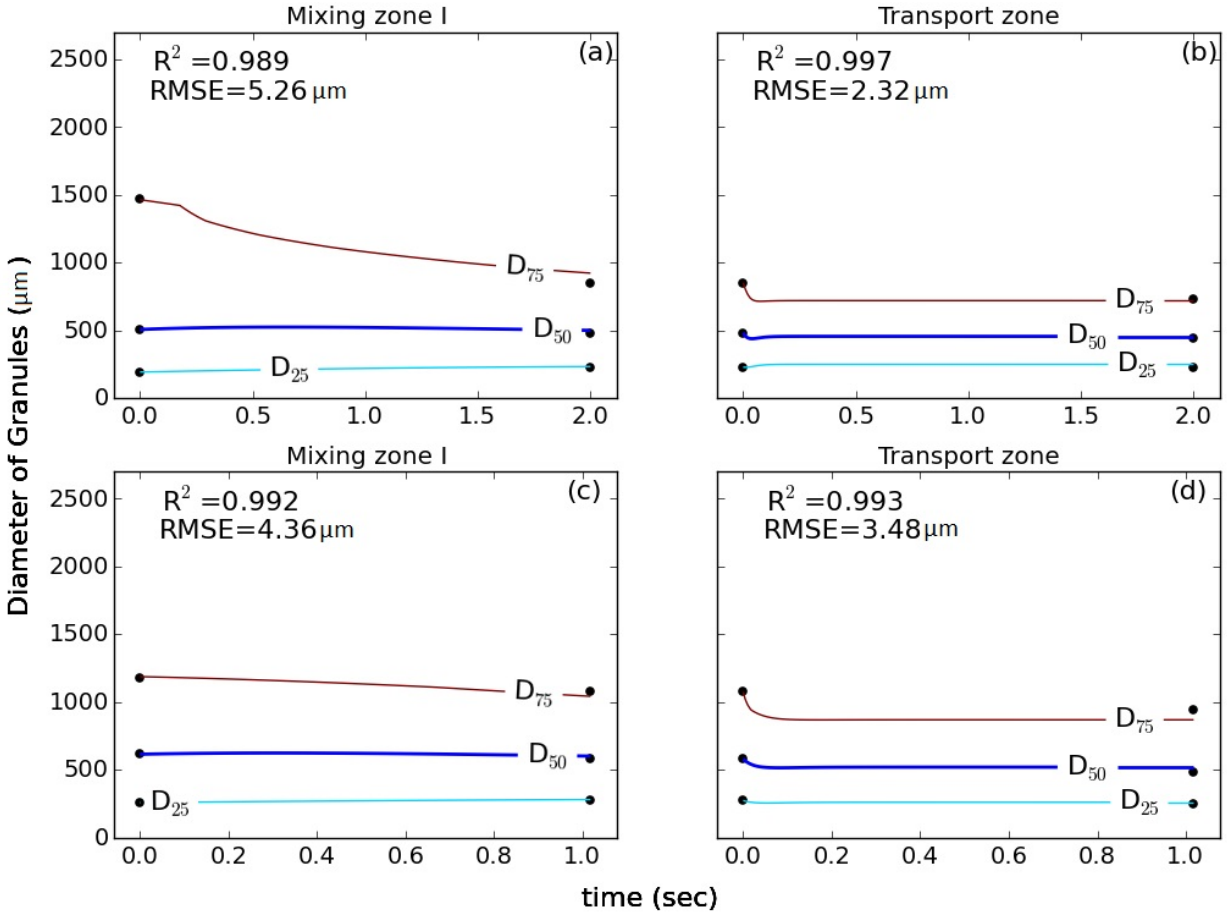

Figure 3: Experimental (•) and simulated (—) trends for dynamic changes in quartiles of the GSD (D_{25}, D_{50}, D_{75}) at low (a and b) and high (c and d) screw speeds for the mixing zone (a and c) and transport zone (b and d) of the TSG.

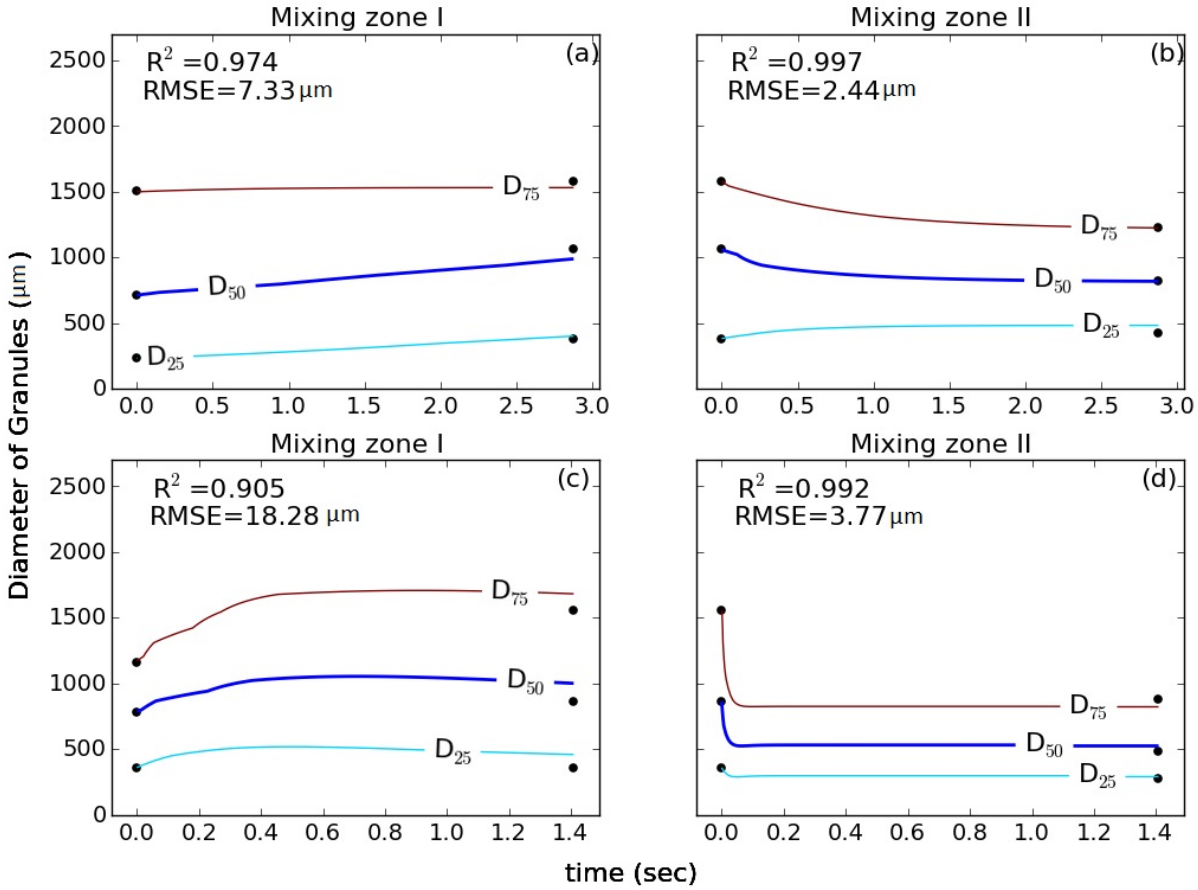

Figure 4: Experimental (•) and simulated (—) trends for dynamic changes in quartiles of the GSD (D_{25}, D_{50} and D_{75}) at low (a and b) and high (c and d) screw speeds for first (a and c) and second (b and d) mixing zones of the TSG.